

Dynamical vertex approximation — a step beyond dynamical mean field theory

A. Toschi^a, A. A. Katanin^{a,b}, and K. Held^a

^aMax-Planck-Institut für Festkörperforschung, 70569 Stuttgart, Germany

^bInstitute of Metal Physics, 620219 Ekaterinburg, Russia

(Dated: Version 8, February 6, 2008)

We develop a diagrammatic approach with local and nonlocal self-energy diagrams, constructed from the local irreducible vertex. This approach includes the local correlations of dynamical mean field theory and long-range correlations beyond. It allows for example to describe (para-)magnons and weak localization effects—in strongly correlated systems. As a first application, we study the interplay between nonlocal antiferromagnetic correlations and the strong local correlations emerging in the vicinity of a Mott-Hubbard transition.

PACS numbers: 71.27.+a, 71.10.Fd

I. INTRODUCTION

Strongly correlated electron systems represent both an opportunity and a challenge for modern physics: An opportunity, since fascinating phenomena occur such as high-temperature superconductivity in cuprates, “colossal” magnetoresistance in manganites, and quantum critical behavior in heavy Fermion compounds. But at the same time they are a challenge, since the very same correlations which are responsible for these phenomena make a theoretical understanding and hence an experimental optimization of these effects particularly difficult.

One of the key issues which arises due to strong electronic correlations and which cannot be described by perturbation theory is the Mott-Hubbard metal-insulator transition.¹ In this respect, dynamical mean field theory (DMFT)^{2,3} was a big step forward to a more thorough understanding of this transition. DMFT becomes exact in the limit of high spatial dimensions ($d \rightarrow \infty$) and already accounts for a large (local) part of electronic correlations—the part which provides for the radical changes upon going from a metal to a Mott-insulator. Real physical systems are however one-, two-, or three-dimensional. Hence, nonlocal correlations, which are neglected in DMFT, may be of importance. Corrections of order $1/d$ have been considered in Ref. 4, resulting in a two-impurity problem, and account for short-range correlations. There has also been recent progress to go beyond DMFT through cluster extensions,⁵ which include correlations within the cluster. These correlations are also necessarily short-range in nature due to numerical limitations of the cluster size.⁶

Often, however, long-range correlations are of vital importance. They are responsible for a rich variety of phenomena, ranging from magnons and screening of the Coulomb interaction to quantum criticality. Long-range correlations are also generally pivotal in the vicinity of phase transitions. The existing theories describing long-range (e.g., magnetic) correlations such as the fluctuation exchange approximation⁷, the two-particle self-consistent approximation⁸, and the functional renormalization group⁹ are restricted to the weak-coupling regime. For strongly correlated systems, e.g., in the vicinity of

a Mott-Hubbard transition, an extension of DMFT by nonlocal (particularly long-range) correlations is hence needed.

For *static* mean-field theories, such corrections have been studied since decades, e.g., for localized¹⁰ and itinerant magnets;^{11,12} for disordered systems such nonlocal effects have also been considered.¹³ But there have been only a very few attempts so far to include long-range correlations beyond dynamical mean field theory: The DMFT self-energy was supplemented by an “external” \mathbf{k} -dependent self-energy which describes spin fluctuations in the spin-fermion model¹⁴ or which stems from the self-consistent renormalization theory,¹⁵ and one might also subsume the GW+DMFT approach¹⁶ here. Let us also note the extended DMFT (E-DMFT¹⁷), which considers the effect of *non-local* interactions on the purely *local* self-energy.

In this paper, we aim at a systematic diagrammatic extension of DMFT by long-range correlations and at an investigation of their effect on the *non-local* self-energy. Diagrammatically, DMFT corresponds to all topologically distinct, but *local* Feynman diagrams for the self-energy. On the next level we assume the locality of the fully irreducible two-particle vertex, and consider all (local or nonlocal) self-energy diagrams which can be constructed from this vertex. One might generalize this approach, requiring locality of the fully irreducible n -particle vertex. Then, one has DMFT for $n = 1$, the dynamical vertex approximation (DFA) for $n = 2$, and the exact solution for $n \rightarrow \infty$. We think however that the one- and two-particle levels ($n = 1, 2$) are the most relevant approximations. If one is interested in a specific physical problem, a restriction of DFA to certain ladder diagrams is reasonable. In the particle-hole channels the ladder diagrams yield (para-)magnons¹¹ and RPA screening; in the particle-particle channel the cooperon diagrams are responsible for attractive pairing interactions and weak localization effects. DFA includes such ladder diagrams beyond DMFT, but with the local vertex instead of the bare interaction so that strong correlations are accounted for.

In this paper we introduce DFA and apply it for studying long-range antiferromagnetic fluctuations in the

three-dimensional Hubbard model. The interplay of these nonlocal spin fluctuations with the local DMFT fluctuations is surprising: Close to the metal-insulator transition the nonlocal fluctuations strongly suppress the spectral function, in contrast to the weak-coupling expectation for three dimensions.¹⁸

The plan of the paper is the following: In Sec. II, we introduce the DGA. Specifically, we derive the full DGA scheme based on the parquet equations in Sec. II A, and a simplified version based on a ladder subset of diagrams in Sec. II B. The latter yields the most important diagrams for the specific problem considered in this paper, i.e., the paramagnon fluctuations in the proximity of the AF transition. We compare this approach with the $1/d$ expansion in Sec. II C. The details concerning the calculation of the local vertex within an exact diagonalization impurity solver are reported in Sec. III (and in the Appendix). Results for the local irreducible vertex and the DGA self-energy and spectral functions are presented in Secs. IV A and IV B respectively. Finally we give a conclusion and discuss the potential of our new method in Sec. V.

II. DYNAMICAL VERTEX APPROXIMATION

Starting point of our considerations is the Hubbard model on a cubic lattice

$$H = -t \sum_{\langle ij \rangle \sigma} c_{i\sigma}^\dagger c_{j\sigma} + U \sum_i n_{i\uparrow} n_{i\downarrow} \quad (1)$$

where t denotes the hopping amplitude between nearest-neighbors, U the Coulomb interaction, $c_{i\sigma}^\dagger$ ($c_{i\sigma}$) creates (annihilates) an electron with spin σ on site i , $n_{i\sigma} = c_{i\sigma}^\dagger c_{i\sigma}$. In the following, we restrict ourselves to the paramagnetic phase with n electrons/site and temperature T .

Let us suppose we know the two-particle vertex $\Gamma_{\mathbf{k}\mathbf{k}'\mathbf{q}}^{\nu\nu'\omega\uparrow\downarrow}$. Then, we can calculate the (nonlocal) self-energy through the exact relation (following from the equation of motion; see Fig. 1a and, e.g., Refs. 20,21)

$$\Sigma_{\mathbf{k},\nu} = U \frac{n}{2} - T^2 U \sum_{\substack{\nu' \omega \\ \mathbf{k}' \mathbf{q}}} \Gamma_{\mathbf{k}\mathbf{k}'\mathbf{q}}^{\nu\nu'\omega\uparrow\downarrow} G_{\mathbf{k}+\mathbf{q},\nu+\omega} G_{\mathbf{k}+\mathbf{q},\nu+\omega} \quad (2)$$

where $G_{\mathbf{k},\nu} = (i\nu_n - \epsilon_{\mathbf{k}} + \mu - \Sigma_{\mathbf{k},\nu})^{-1}$ is the nonlocal Green function, $\epsilon_{\mathbf{k}} = -2t \sum_{\alpha=x,y,z} \cos k_\alpha$ the bare electronic dispersion, and μ the electronic chemical potential. Generally, $\Gamma_{\mathbf{k}\mathbf{k}'\mathbf{q}}^{\nu\nu'\omega\uparrow\downarrow}$ can be expressed diagrammatically, e.g., by taking the fully two-, three- and more particle irreducible local vertices as building blocks and connecting these blocks by local and nonlocal Green functions.

A. Parquet equations

In the DGA, we restrict ourselves to the local fully-irreducible two-particle vertices $\Gamma_{\text{fir}}^{\text{loc}}$. From these build-

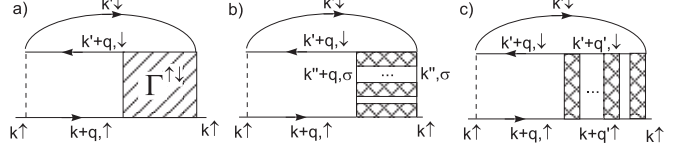


FIG. 1: a) From the reducible vertex we directly obtain the self-energy. b) and c) The two particle-hole channels contributing to the self-energy (longitudinal and transversal) in the ladder approximation. Instead of the bare interaction, ladder diagrams are constructed from the irreducible local vertices (crosshatched) in DGA.

ing blocks, the reducible vertices $\Gamma_{\mathbf{k}\mathbf{k}'\mathbf{q}}^{\nu\nu'\omega\uparrow\downarrow}$ can be obtained through the self-consistent solution of the parquet equations.^{19,20} Representing this vertex as a sum of contributions of different channels, one has^{19,20,21}

$$\Gamma_{\mathbf{k}\mathbf{k}'\mathbf{q}}^{\nu\nu'\omega\uparrow\downarrow} = \Gamma_{\text{fir},\text{loc}}^{\nu\nu'\omega\uparrow\downarrow} + C_{\mathbf{k}\mathbf{k}'\mathbf{q}}^{\nu\nu'\omega} + Z_{\mathbf{k}\mathbf{k}'\mathbf{q}}^{\nu\nu'\omega} + \tilde{Z}_{\mathbf{k}\mathbf{k}'\mathbf{q}}^{\nu\nu'\omega} \quad (3)$$

$$\Gamma_{\mathbf{k}\mathbf{k}'\mathbf{q}}^{\nu\nu'\omega\uparrow\downarrow} = \Gamma_{\mathbf{k}\mathbf{k}'\mathbf{q}}^{\nu\nu'\omega\uparrow\downarrow} - \bar{\Gamma}_{\mathbf{k}\mathbf{k}'\mathbf{q}}^{\nu\nu'\omega\uparrow\downarrow}. \quad (4)$$

Here, $\bar{\Gamma}_{\mathbf{k}\mathbf{k}'\mathbf{q}}^{\nu\nu'\omega\uparrow\downarrow} = \Gamma_{\mathbf{k},\mathbf{k}+\mathbf{q},\mathbf{k}-\mathbf{k}'}^{\nu,\nu+\omega,\nu-\nu'\uparrow\downarrow}$ and the contribution of the three channels can be written in the following form (see Fig. 2)

$$C_{\mathbf{k}\mathbf{k}'\mathbf{q}}^{\nu\nu'\omega} = \Gamma^{\uparrow\downarrow} * G * G * (\Gamma_{\text{fir},\text{loc}}^{\uparrow\downarrow} + Z + \tilde{Z}) \quad (5)$$

$$Z_{\mathbf{k}\mathbf{k}'\mathbf{q}}^{\nu\nu'\omega} = \Gamma^{\uparrow\downarrow} * G * G * (\Gamma_{\text{fir},\text{loc}}^{\uparrow\downarrow} + C + \tilde{Z}) \quad (6)$$

$$\begin{aligned} \tilde{Z}_{\mathbf{k}\mathbf{k}'\mathbf{q}}^{\nu\nu'\omega} = & (\Gamma^{\uparrow\uparrow} + \Gamma^{\downarrow\downarrow}) * G * G * (\Gamma_{\text{fir},\text{loc}}^{\uparrow\downarrow} + C + Z) \\ & - \Gamma^{\uparrow\downarrow} * G * G * (\bar{\Gamma}_{\text{fir},\text{loc}}^{\uparrow\downarrow} + \bar{C} + \bar{Z}) \end{aligned} \quad (7)$$

where * stands for multiplication and summation over the momenta and frequencies given in Fig. 2.

For determining the fully irreducible local vertex $\Gamma_{\text{fir}}^{\text{loc}}$, which is constructed from purely local Feynman diagrams only, we resort to the Anderson impurity model (AIM)²². In fact, the AIM has only one interacting site, so it yields the same local diagrams -and hence the same irreducible vertex- provided that the local Green function is identical. Hence a practical way to obtain $\Gamma_{\text{fir}}^{\text{loc}}$ is through the (e.g., numerical) solution of the AIM. Starting point can be the (local) spin and charge susceptibility of the AIM

$$\chi_{s(c),\text{loc}}^{\nu\nu'\omega} = \chi_{\text{loc}}^{\nu\nu'\omega,\uparrow\downarrow} + \chi_{\text{loc}}^{\nu\nu'\omega,\uparrow\downarrow} \quad (8)$$

from which we can obtain the full (reducible) local vertex $\Gamma_{s(c),\text{loc}}$ and the irreducible local vertices in the spin-, charge- and particle-particle channel ($\Gamma_{s,\text{ir}}$, $\Gamma_{c,\text{ir}}$ and $\Gamma_{pp,\text{ir}}$, respectively) via the standard relations:

$$\chi_{s(c),\text{loc}}^{\nu\nu'\omega} = \chi_{0\omega,\text{loc}}^{\nu} \delta_{\nu\nu'} + \chi_{0\omega,\text{loc}}^{\nu} \Gamma_{s(c),\text{loc}}^{\nu\nu'\omega} \chi_{0\omega,\text{loc}}^{\nu'} \quad (9)$$

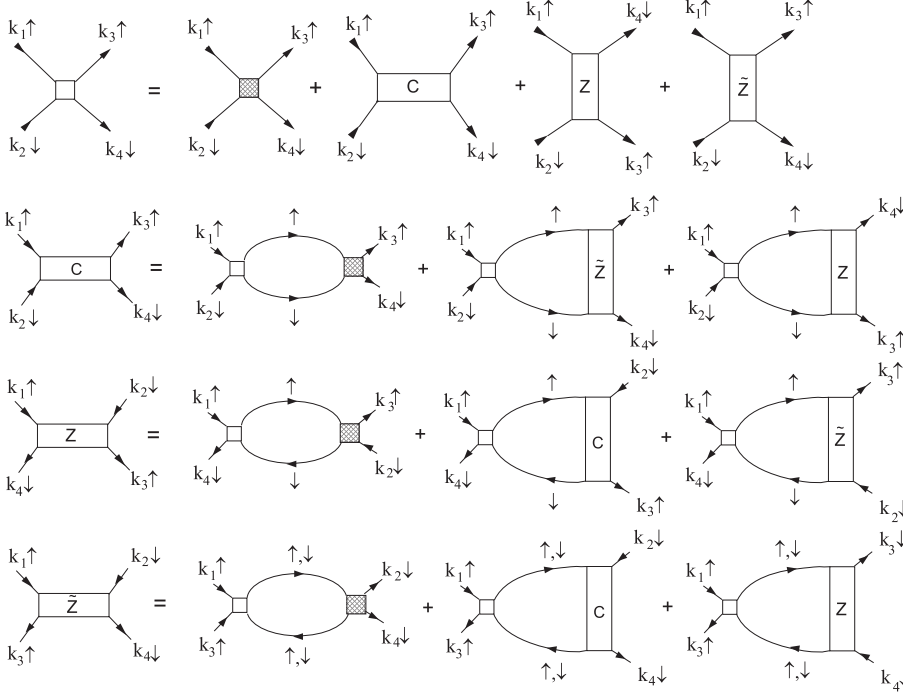
$$\Gamma_{s(c),\text{loc}}^{\nu\nu'\omega} = [(\Gamma_{s(c),\text{ir}}^{\nu\nu'\omega})^{-1} - \chi_{0\omega,\text{loc}}^{\nu'} \delta_{\nu\nu'}]^{-1}, \quad (10)$$

$$\Gamma_{pp,\text{loc}}^{\nu\nu'\omega,\uparrow\downarrow} = [(\Gamma_{pp,\text{ir}}^{\nu,\nu',\tilde{\nu}-\nu})_{\nu,\tilde{\nu}}^{-1} - \Pi_{0\tilde{\nu}+\nu',\text{loc}}^{\tilde{\nu}} \delta_{\nu\tilde{\nu}}]_{\tilde{\nu}=\nu+\omega}^{-1} \quad (11)$$

where

$$\chi_{0\omega,\text{loc}}^{\nu'} = -T G_{\text{loc}}(\nu') G_{\text{loc}}(\omega + \nu'),$$

$$\Pi_{0\omega,\text{loc}}^{\nu'} = T G_{\text{loc}}(\nu') G_{\text{loc}}(\omega - \nu'). \quad (12)$$



From these vertices we can in turn calculate the fully irreducible vertex as

$$\begin{aligned} \Gamma_{\text{fir,loc}}^{\nu\nu'\omega,\uparrow\downarrow} &= \frac{1}{2}(\Gamma_{s,\text{ir}}^{\nu\nu'\omega} - \Gamma_{c,\text{ir}}^{\nu\nu'\omega}) + \Gamma_{s,\text{ir}}^{\nu,\nu+\omega,\nu'-\nu} \\ &\quad + \Gamma_{\text{pp,ir}}^{\nu\nu'\omega} - 2\Gamma_{\text{loc}}^{\nu\nu'\omega\uparrow\downarrow}. \end{aligned} \quad (13)$$

B. Ladder approximation

In this paper, we are particularly interested in paramagnon contributions affecting the self energy in the vicinity of the antiferromagnetic phase. Hence, as discussed in the introduction and with some justification in $1/d$ (see Sec. II C), we restrict ourselves to the ladder subset of the parquet diagrams in the two particle-hole channels shown in Fig. 1b and 1c. These diagrams can be derived from the general parquet set of diagrams of Fig. 2, supposing the locality of C, Z, \tilde{Z} in the r.h.s. of Eqs. (5)-(7). Expressing the ladder diagrams through the vertices in the spin (s) and charge (c) channels $\Gamma_{s(c),\mathbf{q}}^{\nu\nu'\omega}$, which depend on the momentum transferred \mathbf{q} only, the sum of the vertices of Fig. 1b and 1c is obtained as

$$\begin{aligned} \Gamma_{\mathbf{k}\mathbf{k}'\mathbf{q}}^{\nu\nu'\omega,\uparrow\downarrow} &= \frac{1}{2}(\Gamma_{s,\mathbf{q}}^{\nu\nu'\omega} - \Gamma_{c,\mathbf{q}}^{\nu\nu'\omega}) + \Gamma_{s,\mathbf{k}'-\mathbf{k}}^{\nu,\nu+\omega,\nu'-\nu} \\ &\quad - \frac{1}{2}(\Gamma_{s,\text{loc}}^{\nu\nu'\omega} - \Gamma_{c,\text{loc}}^{\nu\nu'\omega}). \end{aligned} \quad (14)$$

Here, the first two terms of Eq. (14) describe the longitudinal and transverse paramagnons in Fig. 1b and 1c, respectively, and the last term subtracts the double-counted local contribution. Note that the nonlocal contribution of the particle-particle channel to the self-

FIG. 2: Graphical notation of the parquet Eqs. (3), (5), (6), and (7). C , Z , and \tilde{Z} denote the contributions of the particle-particle, particle-hole and interaction channels to the non-local vertex $\Gamma_{\mathbf{k}_1,\mathbf{k}_4,\mathbf{k}_3-\mathbf{k}_1}^{\nu_1,\nu_4,\nu_3-\nu_1,\uparrow\downarrow}$ (the momentum and frequency \mathbf{k}_2, ν_2 are determined by conservation laws).

energy, which is not relevant near magnetic instabilities, has been neglected here.

The quantities on the right hand side of Eq. (14) are calculated from the local vertex $\Gamma_{s(c),\text{ir}}^{\nu\nu'\omega}$, irreducible in the spin (charge) channel, via

$$\Gamma_{s(c),\mathbf{q}}^{\nu\nu'\omega} = [(\Gamma_{s(c),\text{ir}}^{\nu\nu'\omega})^{-1} - \chi_{0\mathbf{q}\omega}^{\nu'} \delta_{\nu\nu'}]^{-1}, \quad (15)$$

where $\chi_{0\mathbf{q}\omega}^{\nu'} = -T \sum_{\mathbf{k}} G_{\mathbf{k},\nu'} G_{\mathbf{k}+\mathbf{q},\nu'+\omega}$ with $G_{\mathbf{k},\nu} = [i\nu - \epsilon_{\mathbf{k}} + \mu - \Sigma_{\text{loc}}(\nu)]^{-1}$, Σ_{loc} being the local (DMFT) self-energy. Note that contrary to the full parquet solution in Sec. II A the self-energy of the internal Green functions is considered purely local in accordance with the assumption of the locality of the vertex $\Gamma_{s(c),\text{ir}}^{\nu\nu'\omega}$. The results of this non-self-consistent approach are expected to be close to those of the self-consistent one, due to the cancellations between (self-consistent) non-local self-energy and corresponding corrections to the vertex $\Gamma_{s(c),\text{ir}}$, cf. Ref. 23.

Substituting Eq. (14) into Eq. (2), we obtain after a shift of the momenta and frequencies

$$\begin{aligned} \Sigma_{\mathbf{k},\nu} &= \frac{1}{2}Un + \frac{1}{2}TU \sum_{\nu'\omega,\mathbf{q}} \chi_{0\mathbf{q}\omega}^{\nu'} \left(3\Gamma_{s,\mathbf{q}}^{\nu\nu'\omega} - \Gamma_{c,\mathbf{q}}^{\nu\nu'\omega} \right. \\ &\quad \left. + \Gamma_{c,\text{loc}}^{\nu\nu'\omega} - \Gamma_{s,\text{loc}}^{\nu\nu'\omega} \right) G_{\mathbf{k}+\mathbf{q},\nu+\omega}. \end{aligned} \quad (16)$$

Eq. (16) reduces to the DMFT self-energy if the nonlocal quantities are replaced by local ones. But beyond that, it describes the nonlocal ladder diagrams of Fig. 1b and 1c.

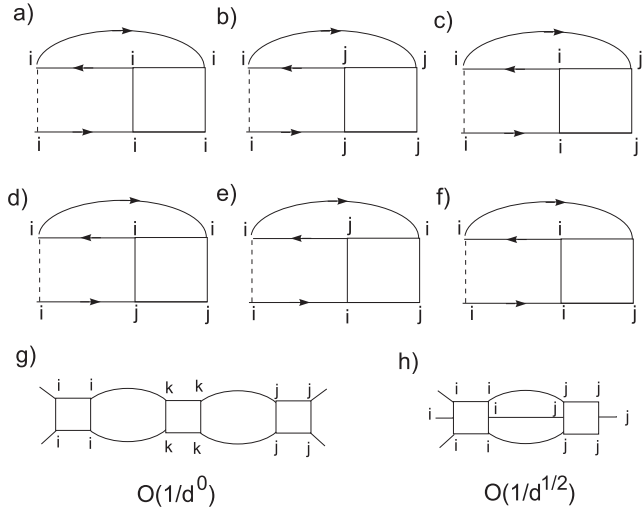


FIG. 3: Diagrams for the self-energy in terms of the vertex to order $1/d^0$, [diagram a), i.e., DMFT] and $1/d^{1/2}$ [diagrams b)-f)]. The ladder diagram g) show how diagrams b)-e) can be constructed from a fully irreducible local two-particle vertex. In contrast, for diagram f) a local three-particle vertex is needed, see h). Hence the contribution f) is the only one not included in the DFA.

C. Comparison to the $1/d$ expansion

Let us compare the result Eq. (16) to that of the $1/d$ expansion. While the DMFT self-energy contains the local Green functions and vertex only (Fig. 3a), the leading nonlocal corrections to the self-energy are proportional to $O(1/d^{1/2})$ and the consideration of the diagrams containing two different sites is sufficient at this order.⁴ The possible types of these diagrams for the self-energy are shown in Fig. 3b-3f. The first type of corrections (Fig. 3b) involve the non-local Green functions only. The second type of corrections (Figs. 3c-3e) contains the non-local vertices with two legs at i and two at j sites. To leading (zeroth) order in $1/d$ these vertices can be expressed as a ladder of local vertices connected by the non-local Green functions, as in Fig. 3g. The contributions of Figs. 3b-3e are hence included in the DGA with the ladder approximation, i.e., in Eq. (16). The last type of $1/d^{1/2}$ corrections to the self-energy (Fig. 3f) involve the three-particle local vertex (Fig. 3h) (and are of order $(U/t)^5$). According to the classification of the introduction, these corrections should be taken into account on the next level of approximation beyond DGA and are the only $1/d^{1/2}$ corrections neglected in DGA. Therefore, the DGA reproduces correctly the leading $1/d$ correction to the self-energy with the three-particle local vertex neglected.

III. CALCULATION OF THE LOCAL FOUR-POINT VERTEX

The calculation of the self-energy (16) requires the knowledge of the local vertex, either fully irreducible—for the general scheme—, or irreducible in the spin (charge) channel—for the ladder diagrams of Fig. 1b and 1c [Eq. (16)]. As already noted, this local vertex can be obtained numerically from the Anderson impurity model. For obtaining the four-point vertex $\Gamma_{s(c),\text{loc}}^{\nu'\nu\omega}$, we need to calculate the AIM susceptibility for three Matsubara frequencies²⁴

$$\begin{aligned} \chi_{loc}^{\nu\nu'\omega\sigma\sigma'} &= T^2 \int_0^{1/T} d\tau_1 d\tau_2 d\tau_3 e^{-i\tau_1\nu} e^{i\tau_2(\nu+\omega)} e^{-i\tau_3(\nu'+\omega)} \\ &\times \left[\langle T_\tau c_{i\sigma}^\dagger(\tau_1) c_{i\sigma}(\tau_2) c_{i\sigma'}^\dagger(\tau_3) c_{i\sigma'}(0) \rangle \right. \\ &\quad \left. - \langle T_\tau c_{i\sigma}^\dagger(\tau_1) c_{i\sigma}(\tau_2) \rangle \langle T_\tau c_{i\sigma'}^\dagger(\tau_3) c_{i\sigma'}(0) \rangle \right]. \quad (17) \end{aligned}$$

where ν, ν' and ω are the two fermionic and the bosonic (transferred) Matsubara frequency, respectively; $\langle T_\tau \dots \rangle$ indicates the thermal expectation value of the time-ordered operators and the last term represents the non-connected contributions. With a spin (anti-) symmetrization (8) we obtain the corresponding charge and spin susceptibilities $\chi_{s(c),\text{loc}}^{\nu\nu'\omega}$. From these, we can either determine the fully irreducible local vertex and through the parquet equations the reducible vertex and the self energy along the lines of Eqs. (13), (3), and (2); or we can directly calculate the particle-hole ladders along the lines of Eqs. (14) and (16). We implement the latter by (i) solving the DMFT equations using exact diagonalization (ED), (ii) calculating via Eq. (17) the local vertices, and (iii) constructing from these through Eq. (16) the DGA self-energy. In principle, this k -dependent self-energy yields new Green functions and a new vertex. However, because of the ladder approximation, we do not perform such a self-consistent calculation here.

Within ED, the calculation of χ_{loc} [Eq. (17)] is straightforwardly (albeit lengthy) performed by resorting to its Lehmann representation, whose explicit expression is reported in the Appendix. The Lehmann representation of χ_{loc} requires four summations over all the Hilbert states of the discretized AIM (compared with only two summations for evaluating the local Green function). This is the higher computational cost of DFA compared with DMFT. By performing a parallel computation of χ_{loc} , we were able to calculate AIMs with $N_s = 5$ sites and evaluate χ_{loc} for the lowest $N_{max} = 20$ (or, in some cases, 25) Matsubara frequencies. This turned out to be sufficient for getting a stable analytic continuation of Eq. (16), using the Padé algorithm. For the momentum summation of Eq. (16) we have used $N_k = 96$ points for each directions.

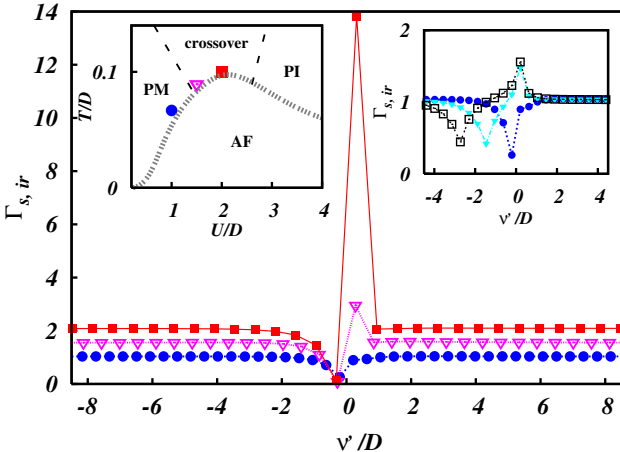


FIG. 4: (Color online) Dependence of the local vertex $\Gamma_{s,ir}^{\nu=\pi T, \nu', \omega=0}$ on the incoming Fermionic frequency ν' , for the three different values of U and T indicated as symbols in the left inset, which shows the DMFT phase diagram with paramagnetic metallic (PM), insulating (PI), and antiferromagnetic (AF) phase. Right inset: Same as main panel but at fixed $U = 1D$ and at different ω 's (circles: $\omega = 0$; triangles: $\omega = 6\pi T$; squares: $\omega = 12\pi T$).

IV. RESULTS

A. Local vertex close to a Mott-Hubbard transition

First, we discuss our results for the local irreducible vertex. Since we are mainly interested in long-range antiferromagnetic fluctuations, we consider temperatures slightly above the DMFT Néel temperature (see the inset of Fig. 4). In this case the largest contribution to the non-local part of the DGA self-energy stems from the terms of Eq. (16) proportional to the local vertex irreducible in the spin channel, particularly with zero bosonic frequency.

In Fig. 4, we show the $\Gamma_{s,ir}^{\nu=\pi T, \omega=0}$ as a function of ν' (with ν fixed to its lowest value πT) at half-filling for three different values of the Hubbard interaction ($U = 1D$, $U = 1.5D$ and $U = 2D$, where $D = 2\sqrt{6}t$ is twice the variance of the non-interacting density of states) and temperature ($T = 0.067D$, $0.089D$ and $0.1D$). This choice allows us to highlight the remarkable differences occurring when moving from the metallic regime to the crossover region of the DMFT phase-diagram of the Hubbard model. In particular, we note that $\Gamma_{s,ir}$ correctly approaches the corresponding value of the bare interaction U for large ν' . On the other hand, at small ν' we observe a radically different behavior of the local vertex depending on the U value: At $U = 1D$, $\Gamma_{s,ir}$ displays a smooth minimum in the region of small ν' , while at $U = 1.5D$ (and even more at $U = 2D$) a very pronounced maximum of $\Gamma_{s,ir}$ appears at $\nu' = \nu$. While the behavior of $\Gamma_{s,ir}$ at small U can be easily interpreted as the screening of the bare interaction, typical of the metallic phase, the huge maximum of $\Gamma_{s,ir}$ at larger U stems from particle-hole fluctuations in the

vicinity of the metal-insulator transition, as discussed in Ref. 21.

B. DGA self-energy and spectral function

The striking behavior of $\Gamma_{s,ir}$ has consequences for the DGA self-energy on the real axis and spectral function, presented in Fig. 5 for the same three different U 's and T 's of Fig. 4 (left inset).

At $U = 1D$, i.e., in the metallic regime of the phase diagram, DMFT shows a quasiparticle peak which is only weakly damped for \mathbf{k} -vectors on the Fermi surface. In DGA, the quasiparticle scatters at nonlocal antiferromagnetic fluctuations, resulting in a broadening of the quasiparticle with a now significant damping given by $\text{Im}\Sigma_{\mathbf{k}}(0)$. For this U value, the distinct features of $\Gamma_{s,ir}$ are not yet particularly pronounced in Fig. 4. It is the strongly enhanced antiferromagnetic susceptibility close to the Néel temperature which leads to this damping in Eq. (16). Stronger damping effects can be observed, studying the Hubbard model in $d = 2$, e.g. by means of the cluster extensions of DMFT⁵, which predict a pseudogap opening at low temperatures. Actually, a stronger damping in $d = 2$ than in the three dimensional case considered here is expected from weak coupling perturbation theory. Unfortunately, to our knowledge, no cluster-DMFT calculation has been performed for the case of $d = 3$, since it poses severe constraints on the cluster size.

At $U = 2D$, the stronger electronic correlation reflects in more pronounced changes of the spectral function. Now, it is the huge $\Gamma_{s,ir}$ of Fig. 4 which strongly suppresses the spectral weight at the Fermi level. This weight is transferred to the Hubbard subbands, which get some additional structure as an effect of magnetic fluctuations. The nonlocal fluctuations result in a much more insulating solution, albeit the Green function is still non-local²⁵.

We emphasize that the mechanism of spectral weight suppression at $U = 2D$ is very different from that in the weak-coupling regime (Ref. 18 and our $U = 1D$ results), where long-range magnetic fluctuations in the immediate vicinity of the magnetic phase transition play the key role. In contrast at $U = 2D$, already relatively short-range spin fluctuations are important because of the strong correlations reflected in the enhanced $\Gamma_{s,ir}$. The spectral weight suppression is therefore also quite robust upon increasing T , i.e., upon going further away from the antiferromagnetic transition (not shown).

At $U = 1.5D$, we have something in between the two cases discussed above: The vertex is already enhanced, but long-range antiferromagnetic fluctuations are still essential. This leads to a suppression of the quasiparticle weight and structured Hubbard bands. Altogether this shows that scattering at nonlocal fluctuations close to a strongly correlated antiferromagnet is very different from that in the vicinity of a weakly correlated Slater antifer-

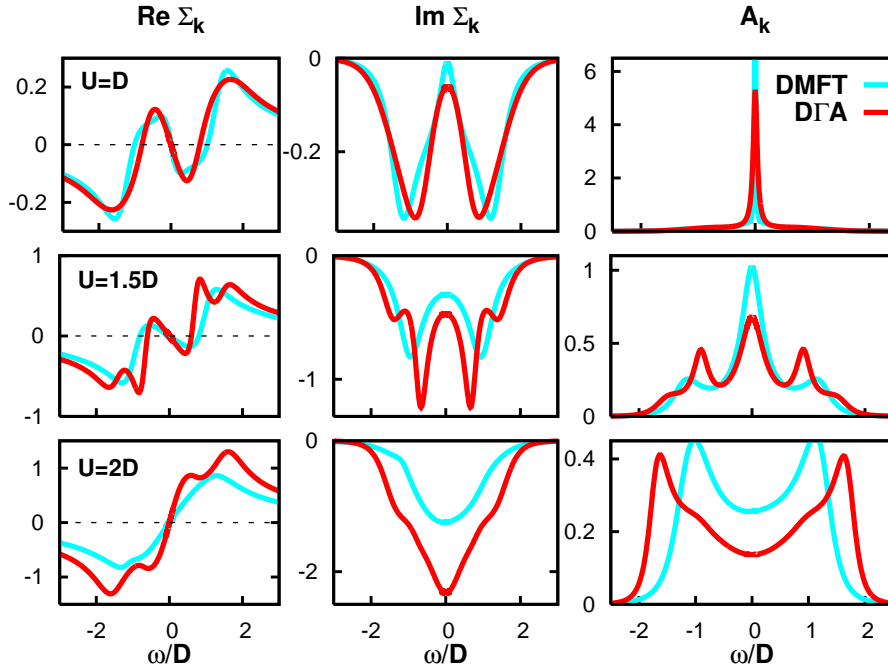


FIG. 5: (Color online) Self energy (left: real, middle: imaginary part) and spectral function (right) at $\mathbf{k} = (\pi/2, \pi/2, \pi/2)$, $U = 1D$ (top), $1.5D$ (central), and $2D$ (bottom) and the same T 's of Fig. 4. Compared to DMFT (light blue line) quasiparticles are damped through scattering at nonlocal spin fluctuations in DΓA (dark red line), and the system is more insulating. At $U = 1.5D$ and $2D$, these effects are drastically enhanced because of strong local correlations reflected in $\Gamma_{s,ir}$

romagnet.

V. CONCLUSIONS

We developed the dynamical vertex approximation (DΓA) based on the assumption of the locality of the irreducible vertex. For the half-filled three-dimensional Hubbard model, we found that the local vertex (irreducible in the particle-hole spin channel) strongly depends on all three frequencies; it is hugely enhanced at some particular frequencies for large U . These strong local correlations entail similarly strong nonlocal fluctuations. The scattering of the quasiparticles at these nonlocal spin fluctuations, in turn, drastically reduces their life times; spectral weight is transferred to the Hubbard bands which develop some additional structure. These nonlocal effects of strong electronic correlations are very different from those at weak coupling. It is a strength of DΓA to reveal them.

Including long-range correlations, DΓA opens the door to study a wide variety of physical phenomena, previously described only for weakly correlated systems, such as magnons in strongly correlated (anti-)ferromagnets²⁸, the interplay of weak localization effects and strong electron interactions, and vertex corrections to the RPA screening. A self-consistent realization of the approach might also allow us to study how nonlocal fluctuations suppress magnetic long-range ordering, whether anti-ferromagnetic fluctuations in the vicinity of the metal-insulator transition result in unconventional superconductivity, and how physical quantities change in the vicinity of ferro- and antiferromagnetic quantum critical points.

Acknowledgments. We thank W. Metzner, M. Capone, C. Castellani, G. Sangiovanni, and R. Arita for stimulating discussions; we are indebted to M. Capone also for providing the DMFT(ED) code which has served as a starting point. This work was supported by the Deutsche Forschungsgemeinschaft through the Emmy-Noether program (AT,KH) and 436 RUS 113/723/0-2 (AK) and by the Russian Basic Research Foundation through Grant No. 747.2003.2 (AK).

Note added. During the completion of our paper, we learned about a related study, Ref. 26. Another related paper, Ref. 27, has appeared just after our pre-print.

APPENDIX: LEHMANN REPRESENTATION OF THE LOCAL SUSCEPTIBILITY

In this Appendix we report the explicit expression of the Lehmann representation for the local (and spin-dependent) susceptibility, which is necessary for performing the calculation of the basic “brick” of the DΓA (i.e., the local four point vertex) within the ED algorithm (see Sec. III).

We start with the evaluation of the T-ordered product appearing in the definition of the (spin-dependent) local susceptibility in Eq. (17):

$$\tilde{\chi}_{loc}^{\nu\nu'\omega\sigma\sigma'} = T^2 \int_0^\beta d\tau_1 d\tau_2 d\tau_3 e^{-i\tau_1\nu} e^{+i\tau_2(\nu+\omega)} e^{-i\tau_3(\nu'+\omega)} \times \langle T_\tau c_{i\sigma}^\dagger(\tau_1) c_{i\sigma}(\tau_2) c_{i\sigma'}^\dagger(\tau_3) c_{i\sigma'}(0) \rangle$$

$$\begin{aligned}
&= T^2 \int_0^\beta d\tau_1 \left[\int_0^{\tau_1} d\tau_2 \left(\int_0^{\tau_2} d\tau_3 - \int_{\tau_2}^{\tau_1} d\tau_3 + \int_{\tau_1}^\beta d\tau_3 \right) \right. \\
&\quad \left. - \int_{\tau_1}^\beta d\tau_2 \left(\int_0^{\tau_1} d\tau_3 - \int_{\tau_1}^{\tau_2} d\tau_3 + \int_{\tau_2}^\beta d\tau_3 \right) \right] \\
&\quad \times e^{-i\nu(\tau_1-\tau_2)} e^{i\omega(\tau_2-\tau_3)} e^{-i\nu'\tau_3} \langle \dots \rangle \\
&= \frac{T^2}{Z} (\chi_{\text{loc}}^{123} + \chi_{\text{loc}}^{132} + \chi_{\text{loc}}^{312} + \chi_{\text{loc}}^{213} + \chi_{\text{loc}}^{231} + \chi_{\text{loc}}^{321}) \quad (\text{A.1})
\end{aligned}$$

where $\beta = 1/T$, Z is the partition function and with $\langle \dots \rangle$ we indicate the thermal and quantum average of the four fermionic operators in the r.h.s. of the first line

of the equation, which are already ordered in terms of decreasing times (with no further sign change). The six different contributions χ_{loc}^{123} , χ_{loc}^{132} , \dots appearing in the last line of Eq. (A.1) reflect the six different ways of arranging the order of the three Matsubara times τ_1 , τ_2 and τ_3 in the time integral of Eq. (17). χ_{loc}^{123} , χ_{loc}^{132} , \dots can be explicitly expressed in a very convenient way for ED scheme, i.e., in terms of the eigenenergies E_N and the matrix elements $\langle N | c_\sigma^{(\dagger)} | M \rangle = (c_\sigma^{(\dagger)})_{NM}$, of the associated AIM, through the standard Lehmann representation. The evaluation of the six time integrals in Eq. (A.1) is straightforward- albeit lengthy, and yields the following results:

$$\begin{aligned}
\chi_{\text{loc}}^{123} &= \sum_{N,M,L,S} \frac{-1}{i(\nu' + \omega) - E_L + E_S} \left[\frac{1}{i(\nu - \nu') + E_M - E_S} \left(\frac{e^{-\beta E_N} + e^{-\beta E_S}}{i\nu' - E_N + E_S} - \frac{e^{-\beta E_M} + e^{-\beta E_N}}{i\nu - E_N + E_M} \right) \right. \\
&\quad \left. - \frac{1}{i(\nu + \omega) + E_M - E_L} \left(\frac{e^{-\beta E_L} - e^{-\beta E_N}}{i\omega + E_N - E_L} - \frac{e^{-\beta E_M} + e^{-\beta E_N}}{i\nu - E_N + E_M} \right) \right] \times (c_\sigma^\dagger)_{NM} (c_\sigma)_{ML} (c_{\sigma'}^\dagger)_{LS} (c_{\sigma'})_{SN} \quad (\text{A.2})
\end{aligned}$$

$$\begin{aligned}
\chi_{\text{loc}}^{132} &= \sum_{N,M,L,S} \frac{1}{i(\nu' + \omega) - E_M + E_L} \left[\frac{1}{i(\nu + \omega) + E_L - E_S} \left(\frac{e^{-\beta E_N} + e^{-\beta E_S}}{i\nu' - E_N + E_S} + \frac{e^{-\beta E_L} - e^{-\beta E_N}}{i(\nu + \nu' + \omega) - E_N + E_L} \right) \right. \\
&\quad \left. + \frac{1}{i(\nu - \nu') + E_M - E_S} \left(\frac{e^{-\beta E_M} + e^{-\beta E_N}}{i\nu + E_M - E_N} - \frac{e^{-\beta E_S} + e^{-\beta E_N}}{i\nu' + E_S - E_N} \right) \right] \times (c_\sigma^\dagger)_{NM} (c_{\sigma'}^\dagger)_{ML} (c_\sigma)_{LS} (c_{\sigma'})_{SN} \quad (\text{A.3})
\end{aligned}$$

$$\begin{aligned}
\chi_{\text{loc}}^{213} &= \sum_{N,M,L,S} \frac{1}{i(\nu' + \omega) + E_L - E_M} \frac{1}{i(\nu + \omega) + E_S - E_N} \left(\frac{e^{-\beta E_M} - e^{-\beta E_S}}{i\omega + E_S - E_M} + \frac{e^{-\beta E_L} - e^{-\beta E_N}}{i(\nu + \nu' + \omega) - E_N + E_L} \right. \\
&\quad \left. + \frac{e^{-\beta E_M} + e^{-\beta E_N}}{i\nu + E_M - E_N} - \frac{e^{-\beta E_S} + e^{-\beta E_L}}{i\nu' + E_L - E_S} \right) \times (c_\sigma^\dagger)_{NM} (c_{\sigma'}^\dagger)_{ML} (c_{\sigma'})_{LS} (c_\sigma)_{SN} \quad (\text{A.4})
\end{aligned}$$

$$\begin{aligned}
\chi_{\text{loc}}^{231} &= \sum_{N,M,L,S} \frac{-1}{i(\nu' + \omega) + E_M - E_N} \left[\frac{1}{i(\nu - \nu') - E_M + E_S} \left(\frac{e^{-\beta E_M} + e^{-\beta E_L}}{i\nu + E_L - E_M} - \frac{e^{-\beta E_L} + e^{-\beta E_S}}{i\nu' + E_L - E_S} \right) \right. \\
&\quad \left. - \frac{1}{i(\nu + \omega) + E_S - E_N} \left(\frac{e^{-\beta E_L} - e^{-\beta E_N}}{i(\nu + \nu' + \omega) + E_L - E_N} - \frac{e^{-\beta E_L} + e^{-\beta E_S}}{i\nu' + E_L - E_S} \right) \right] \times (c_{\sigma'}^\dagger)_{NM} (c_{\sigma'}^\dagger)_{ML} (c_{\sigma'})_{LS} (c_\sigma)_{SN} \quad (\text{A.5})
\end{aligned}$$

$$\begin{aligned}
\chi_{\text{loc}}^{312} &= \sum_{N,M,L,S} \frac{-1}{i(\nu' + \omega) + E_M - E_N} \frac{1}{i(\nu + \omega) + E_L - E_S} \left(\frac{e^{-\beta E_M} - e^{-\beta E_S}}{i\omega + E_M - E_S} + \frac{e^{-\beta E_L} + e^{-\beta E_M}}{i\nu + E_L - E_M} \right. \\
&\quad \left. - \frac{e^{-\beta E_N} + e^{-\beta E_S}}{i\nu' + E_S - E_N} + \frac{e^{-\beta E_N} - e^{-\beta E_L}}{i(\nu + \nu' + \omega) + E_L - E_N} \right) \times (c_{\sigma'}^\dagger)_{NM} (c_\sigma^\dagger)_{ML} (c_\sigma)_{LS} (c_{\sigma'})_{SN} \quad (\text{A.6})
\end{aligned}$$

$$\begin{aligned}
\chi_{\text{loc}}^{321} &= \sum_{N,M,L,S} \frac{1}{i(\nu' + \omega) + E_M - E_N} \left[\frac{1}{i(\nu + \omega) + E_M - E_L} \left(\frac{e^{-\beta E_S} + e^{-\beta E_L}}{i\nu + E_S - E_L} + \frac{e^{-\beta E_S} - e^{-\beta E_M}}{i\omega + E_M - E_S} \right) \right. \\
&\quad \left. - \frac{1}{i(\nu - \nu') + E_N - E_L} \left(\frac{e^{-\beta E_S} + e^{-\beta E_L}}{i\nu + E_S - E_L} - \frac{e^{-\beta E_S} + e^{-\beta E_N}}{i\nu' + E_S - E_N} \right) \right] \times (c_{\sigma'}^\dagger)_{NM} (c_\sigma)_{ML} (c_\sigma^\dagger)_{LS} (c_{\sigma'})_{SN} \quad (\text{A.7})
\end{aligned}$$

After the DMFT self-consistency condition has been

fulfilled, the ED-DMFT evaluation of the local suscepti-

bility Eq. (17) is obtained directly by plugging the eigenvalues E_N and the matrix elements $(c_\sigma)_{NM}$ of the associated AIM in the Eqs. (A.2)-(A.7) and performing the corresponding four summations over the Hilbert space. The relevant numerical effort related to the Hilbert space summations can be handled by means of a parallel computations for the case considered here (i.e., $N_s = 5$ and $N_{max} \geq 20$). States for which all Boltzmann weights ($e^{-\beta E}$) or matrix elements are smaller than 10^{-6} are neglected.

For the numerical implementation, let us note that

some denominators in Eqs. (A.2)-(A.7), characterized by a bosonic Matsubara frequency (e.g., those with $i\omega$ or with $i(\nu - \nu')$), can vanish during the summations over the Hilbert space.

However there are no divergences, since the corresponding numerators are simultaneously vanishing, so that their limit is always well defined. To avoid computational problems, we simply add a very small energy shift in all the terms with a vanishing denominator (e.g., $E_N \rightarrow E_N + 10^{-8}$), in order to evaluate numerically the correct limiting values.

¹ N. F. Mott, Rev. Mod. Phys. **40**, 677 (1968); *Metal-Insulator Transitions* (Taylor & Francis, London, 1990); F. Gebhard, *The Mott Metal-Insulator Transition* (Springer, Berlin, 1997).

² W. Metzner and D. Vollhardt, Phys. Rev. Lett. **62**, 324 (1989);

³ A. Georges, G. Kotliar, W. Krauth, and M. Rozenberg, Rev. Mod. Phys. **68**, 13 (1996); G. Kotliar and D. Vollhardt, Physics Today **57**, 53 (2004).

⁴ A. Schiller and K. Ingersent, Phys. Rev. Lett. **75**, 113 (1995).

⁵ M. H. Hettler, A. N. Tahvildar-Zadeh, M. Jarrell, T. Pruschke, and H. R. Krishnamurthy, Phys. Rev. B **58**, (1998) 7475; C. Huscroft, M. Jarrell, Th. Maier, S. Moukouri, and A. N. Tahvildarzadeh, Phys. Rev. Lett. **86**, 139 (2001); A. I. Lichtenstein and M. I. Katsnelson, Phys. Rev. B **62**, R9283 (2000); G. Kotliar, S. Y. Savrasov, G. Pálsson, and G. Biroli, Phys. Rev. Lett. **87**, 186401 (2001); T. A. Maier, M. Jarrell, T. Pruschke, M. H. Hettler, Rev. Mod. Phys. **77**, 1027 (2005).

⁶ Cluster sizes can be extended by using e.g. the fluctuation exchange approximation, see K. Aryanpour, M. H. Hettler, and M. Jarrell, Phys. Rev. B **67**, 085101 (2003).

⁷ N. E. Bickers, D. J. Scalapino, and S. R. White, Phys. Rev. Lett. **62**, 961 (1989).

⁸ Y. M. Vilk and A. M. S. Tremblay, J. Phys. I (France) **7**, 1309 (1997).

⁹ D. Zanchi and H. J. Schulz, Phys. Rev. B **54**, 9509 (1996); C. J. Halboth and W. Metzner, Phys. Rev. Lett. **85**, 5162 (2000); C. Honerkamp, M. Salmhofer, N. Furukawa, and T. M. Rice, Phys. Rev. B **63**, 035109 (2001); C. Honerkamp and M. Salmhofer, Phys. Rev. Lett. **87**, 187004 (2001); A. A. Katanin and A. P. Kampf, Phys. Rev. B **68**, 195101 (2003).

¹⁰ V. G. Vaks, A. I. Larkin, and S. A. Pikin, Zh. Eksp. Teor. Phys. **53**, 281 (1967); 1089 (1967) [Sov. Phys. JETP **26**, 188 (1968); 647 (1968)].

¹¹ T. Moriya, “Spin fluctuations in Itinerant Electron Magnetism” (Springer, 1985).

¹² A. Georges and J. S. Yedidia, Phys. Rev. B **43**, 3475 (1991), P. G. J. van Dongen, Phys. Rev. B **50**, 14016 (1994).

¹³ V. Janiš, Phys. Rev. B **64**, 115115 (2001).

¹⁴ E. Z. Kuchinskii, I. A. Nekrasov, and M. V. Sadovskii Sov. Phys. JETP Lett. **82**, 198 (2005); M. V. Sadovskii, I. A. Nekrasov, E. Z. Kuchinskii, Th. Pruschke, and V. I. Anisimov, Phys. Rev. B **72**, 155105 (2005).

¹⁵ T. Saso, J. Phys. Soc. Jpn **68**, 3941 (1999).

¹⁶ S. Biermann, F. Aryasetiawan, and A. Georges, Phys. Rev. Lett. **90**, 086402 (2003).

¹⁷ Q. Si and J.L. Smith, Phys. Rev. Lett., **77**, 3391 (1996). H. Kajueter, Ph.D. thesis, Rutgers University (1996).

¹⁸ J. M. Vilk and A.-M. S. Tremblay J. Phys. I (France) **7**, 1909 (1997).

¹⁹ Y. A. Bychkov, L. P. Gorkov, and I. E. Dzyaloshinskii, Zh. Exp. Teor. Fiz. **50**, 738 (1966) [Sov. Phys. JETP **23**, 489 (1966)].

²⁰ N. E. Bickers and S. R. White, Phys. Rev. B **43**, 8044 (1991).

²¹ V. Janiš, Phys. Rev. B **60** 11345 (1999).

²² For the physics of the AIM see, e.g., P. W. Anderson in *Moment formation in solids*, W. J. L. Buyers (Ed.), (Plenum Press, New York, 1984); A. C. Hewson, *The Kondo Problem to Heavy Fermions*, Cambridge Studies in Magnetism Vol. 2 (Cambridge University Press, Cambridge 1993).

²³ W. Metzner, C. Castellani, and C. Di Castro, Adv. Phys. **47**, 317 (1998).

²⁴ This three frequency vertex has been already introduced in Ref. 3, but, to our knowledge, only the static ($\omega = 0$) vertex has been calculated, and used for computing DMFT static susceptibilities.

²⁵ Let us note that the analytical continuation sometimes also shows a little bump for the U=2D case. But quantitatively the results are very similar.

²⁶ H. Kusunose, J. Phys. Soc. Jpn. **75**, 054713 (2006).

²⁷ C. Slezak, M. Jarrell, Th. Maier, and J. Deisz, cond-mat/0603421 (unpublished).

²⁸ The generalization of the DGA to the case of magnetically ordered phases is straightforward, albeit lengthy: it is necessary to consider different vertices for the longitudinal and transverse spin fluctuations.